Journal of Inorganic and Organometallic Polymers and Materials (2020) 30:4615–4621
https://doi.org/10.1007/s10904-020-01601-x

Fabrication of Ag NPs/Zn-MOF Nanocomposites and Their Application as Antibacterial Agents

Reza Sacourbaravi[1] · Zeinab Ansari-Asl[1] · Mohammad Kooti[1] · Valiollah Nobakht[1] · Esmaeil Darabpour[2]

Received: 27 March 2020 / Revised: 19 May 2020 / Accepted: 20 May 2020 / Published online: 26 May 2020

Abstract
Three new nanocomposites consisting of Zn(II) metal–organic framework (Zn-MOF) and Ag nanoparticles (Ag NPs), designated as Ag NPs/Zn-MOFs **1**–**3**, based on the used doses of $AgNO_3$, were fabricated. FT-IR (Fourier-transform infrared), PXRD (powder X-ray diffraction), SEM (scanning electron microscope), EDS (energy-dispersive X-ray spectroscopy) mapping, and TEM (transmission electron microscope) techniques were used for characterization of the prepared compounds. The obtained results have shown that the Ag NPs were successfully loaded on the Zn-MOF template. The spherical morphology of Ag NPs with diameter of 30–60 nm was confirmed through TEM analysis. The antibacterial activity of the synthesized compounds was then assessed against *Staphylococcus aureus*, *Bacillus subtilis*, *Pseudomonas aeruginosa*, and *Escherichia coli*, using disc diffusion method. Among the studied composites, the one with higher dose of used $AgNO_3$, i.e. Ag NPs/Zn-MOF **1**, had a broad-spectrum of antibacterial activity.

Keywords Silver nanoparticles · Metal–organic Framework · Nanocomposite · Antibacterial activity

1 Introduction

Metal nanoparticles have attracted a lot of interest and have been widely used in industrial, biological, and agricultural fields due to their unique electrical, optical, catalytic, and biological properties [1–3]. Among various metal nanoparticles, silver nanoparticles (Ag NPs) owing to their fascinating features have attracted much attention for their potential applications in various areas, including sensing materials, biomedical devices, and wound dressings [4–6]. Furthermore, due to their cytotoxic effect against various bacteria, Ag NPs can be considered as suitable antibacterial agent [7–9].

However, aggregation of Ag NPs in solution and the difficulty of their recovery are considered as two of the critical challenges for the wide applications of these nanoparticles. Therefore, many strategies were used for overcoming these problems, among them encapsulation and immobilization of Ag NPs into/on various matrices were found to be more desired approaches [10–12].

On the other hand, metal–organic frameworks (MOFs), as porous organic–inorganic hybrids, have been widely applied as templates for immobilization of metal NPs [13–15]. MOFs are crystalline compounds consisting of metal ions and organic linkers. These structures, owing to their interesting properties, such as high porosity, high surface area, and diversity, have attracted much attention. These materials can be considered as promising antibacterial materials due to their large pores size, which can be used to deliver therapeutic agents and their ability to release metal ions [16–18].

There are many studies devoted to the fabrication of MOF's nanocomposites through the application of MOFs as templates for immobilization of metal nanoparticles. Surya et al. deposited Ag NPs onto UiO-66(Zr) metal–organic framework by the impregnation method [19]. Mahugo et al. prepared Ag@MIL-100(Fe) nanocomposites through different procedures [20].

In this work, nano Zn-MOF was synthesized by an ultrasonic method, and Ag NPs were then deposited onto the Zn-MOF surface via reduction of Ag^+ ions by sodium borohydride. The fabricated Ag NPs/Zn-MOF nanocomposites were characterized using FT-IR, PXRD, SEM, TEM, and EDS-mapping techniques. After structural characterization,

✉ Zeinab Ansari-Asl
z.ansari@scu.ac.ir

[1] Department of Chemistry, Faculty of Science, Shahid Chamran University of Ahvaz, Ahvaz, Iran

[2] Department of Biology, Faculty of Science, Shahid Chamran University of Ahvaz, Ahvaz, Iran

the antibacterial activity of the as-prepared compounds was assessed against some pathogenic bacteria.

2 Experimental

2.1 Materials and Methods

Zinc(II) nitrate hexahydrate, 2-Aminoterephthalic acid (2-NH_2-H_2BDC), ammonium sulfate, and triethylamine were obtained from Sigma Aldrich Company and used as received. Dimethylformamide (DMF), chloroform ($CHCl_3$), sodium borohydride ($NaBH_4$), and ethanol were purchased from Merck Company. The ligand 1,4-bis(4-pyridyl)-2,3-diaza-1,3-butadiene (4-bpdb) was prepared according to the previously reported procedure [21]. The FT-IR spectra of the samples were recorded on a Perkin Elmer spectrum two spectrophotometer. PXRD patterns were obtained on the X'Pert PRO powder diffractometer, using CuKα radiation. EDS-mapping and SEM images were taken using TESCAN MIRA3 and LEO 1455VP microscopes. TEM images were recorded with LEO 906E microscope.

2.2 Synthesis of Nano Zn-MOF

4-bpdb (0.21 g, 1.0 mmol) and 2-NH_2-H_2BDC (0.181 g, 1 mmol) were separately dissolved in DMF (4 mL). Then, these solutions were added to a solution of $Zn(NO_3)_2{\cdot}6H_2O$ (0.297 g, 1.0 mmol) in DMF (3 mL) under ultrasonic irradiation. After adding a solution of Et_3N (4 drops) in DMF (4 mL) into the above solution, yellow precipitate was formed. The mixture was sonicated for 90 min. The product was filtered out, washed with DMF and EtOH, and then dried at 60 °C for 24 h in an oven.

2.3 Fabrication of Ag NPs/Zn-MOF Nanocomposites

Ag NPs/Zn-MOF nanocomposites were fabricated through encapsulating of Ag^+ ions into the framework of Zn-MOF and subsequent reduction of these ions. In order to obtain suitable Zn-MOF for loading of Ag NPs, this MOF should be first activated by removing the guest DMF molecules from its framework. Hence, the Zn-MOF was immersed in $CHCl_3$ and stirred for 5 days (the solvent was refreshed every 24 h). Finally, the obtained solid was centrifuged and dried at 80 °C for 24 h. A sample of the activated Zn-MOF (0.1 g) was suspended in EtOH (10 mL) under ultrasonic irradiation. A solution of $AgNO_3$ (0.037 g, 0.22 mmol) in EtOH (10 mL) was added to the above suspension dropwise. The resulted yellow suspension was stirred for 3 h, filtered, and washed several times with distilled water to remove any untreated Ag ions. KCl was used for monitoring the presence of free silver ion in the supernatant solution. Afterward, a solution of $NaBH_4$ (0.1 g, 2.64 mmol) in distilled water (5 mL) was slowly added to the mixture to form Ag NPs/Zn-MOF **1** nanocomposite as a dark powder. The product was then separated, washed with EtOH, and dried at 70 °C for 24 h. Ag NPs/Zn-MOF **2** and Ag NPs/Zn-MOF **3** were also fabricated according to the above-described procedure, using 0.018 and 0.009 g of $AgNO_3$, respectively.

2.4 Antibacterial Activity Assay

Antibacterial activity of the prepared nanocomposites was investigated against the gram-positive strains *Staphylococcus aureus* ATCC 6538 and *Bacillus subtilis* ATCC 6633, as well as the gram-negative strains *Pseudomonas aeruginosa* ATCC 9027 and *Escherichia coli* ATCC 25922, using disc diffusion method. At first, the bacterial suspension (100 µL of a 0.5 McFarland turbidity standard) was uniformly plated on Muller Hinton agar (MHA, Merck) plates. In the next step, four concentrations (1, 2, 4, and 8 mg mL^{-1}) of each of the nanocomposites were prepared. The sterile filter paper discs (6 mm diameter) were saturated by 35 µL of different concentrations of the nanocomposites and then were placed on lawn cultures. The petri dishes were subsequently incubated at 37 °C for 24 h and the inhibition zone around each disc was finally measured in mm.

3 Results and Discussion

3.1 Fabrication and Characterization of Ag NPs/Zn-MOF Nanocomposites

Fabrication of Ag NPs/Zn-MOF nanocomposites was performed through multistep procedure. These involve, synthesis of Zn-MOF, activating of the synthesized Zn-MOF, loading of Ag^+ on Zn-MOF, and finally reducing of Ag^+ ions by $NaBH_4$. The schematic process for the preparation of Ag NPs/Zn-MOF nanocomposites is given in Scheme 1. The obtained nanocomposites were characterized by FTIR, PXRD, SEM, EDS mapping, and TEM techniques.

FT-IR spectra of Zn-MOF and its nanocomposites are shown in Fig. 1. For pure Zn-MOF, the band at 1258 cm^{-1} is assigned to ν(C–N) of the 2-NH_2-BDC^{2-} ligand. The absorption bands at 1384 cm^{-1} and 1576 cm^{-1} are attributed to the vibrations of carboxylate groups. The band occurs at 1608 cm^{-1} is assigned to C=N stretching vibration of the 4-bpdb. The FT-IR spectra of the nanocomposites did not show significant difference from the spectrum of Zn-MOF. The absorptions at 3360 cm^{-1} and 3465 cm^{-1} can be attributed to the vibration of NH_2 groups [22, 23].

The loading of Ag NPs into the Zn-MOF matrix is confirmed by comparison of the PXRD patterns of Zn-MOF and that of the as-fabricated nanocomposites. PXRD

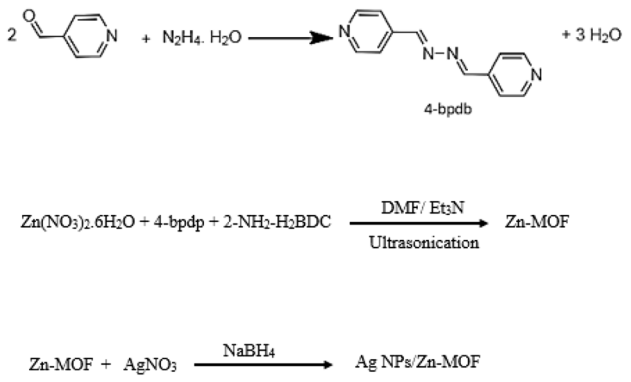

Scheme 1 Schematic representation for the synthesis procedure of Ag NPs/Zn-MOF nanocomposites

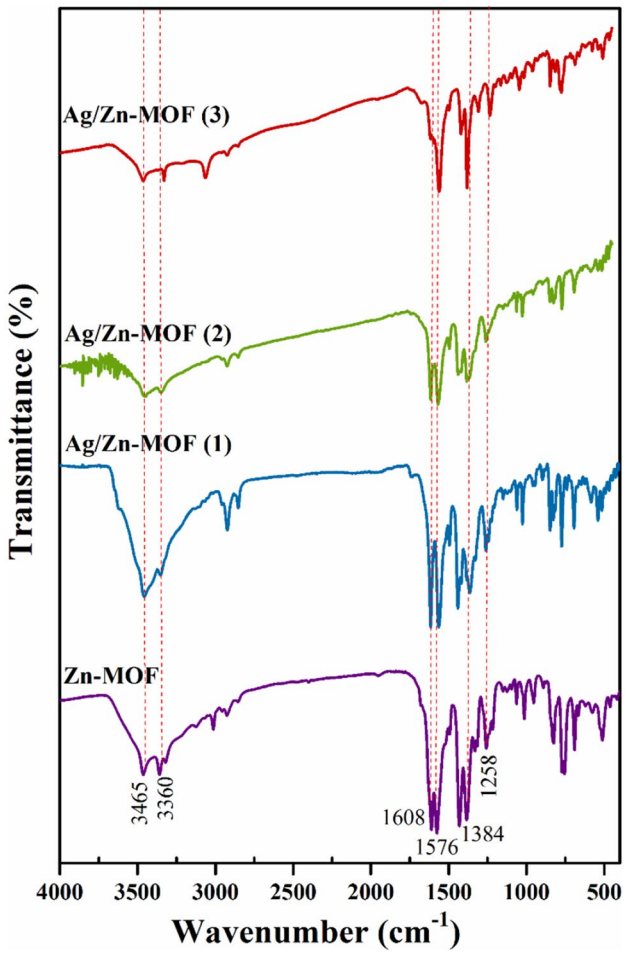

Fig. 1 FT-IR spectra of Zn-MOF and the as-prepared Ag NPs/Zn-MOF nanocomposites, red dotted lines exhibit the characteristic absorption peaks of Zn-MOF (Color figure online)

patterns of the Zn-MOF and Ag NPs/Zn-MOF nanocomposites were shown in Fig. 2. The pure Zn-MOF exhibits

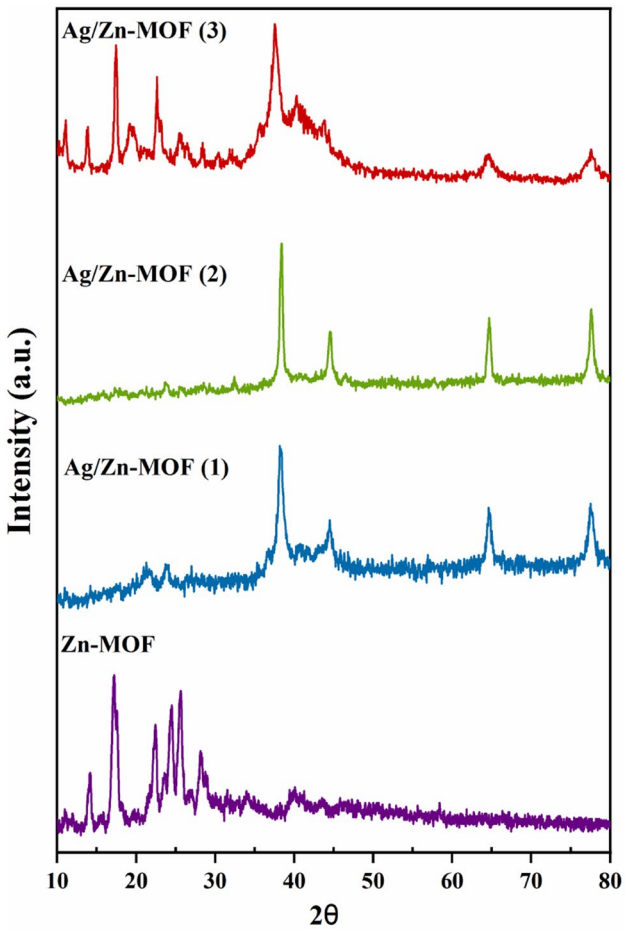

Fig. 2 PXRD patterns of Zn-MOF and Ag NPs/Zn-MOF nanocomposites

characteristic diffraction peaks in agreement with the previous reports [22–24]. PXRD patterns of the Ag NPs/Zn-MOF nanocomposites also exhibited the characteristic peaks of pristine Zn-MOF and other newly revealed peaks at 2θ = 38.3, 44.5, 64.7, and 77.8 which can be respectively attributed to the (111), (200), (220), and (311) lattice planes of Ag NPs [25–27]. This observation demonstrated the reduction of Ag ions and the loading of Ag NPs in/on Zn-MOF.

The morphologies of Ag NPs/Zn-MOF nanocomposites were determined by SEM and TEM (Fig. 3) analyses. These images exhibited that spherical Ag NPs with diameters of 30–60 nm are formed on the surface of the Zn-MOF. EDS mapping was used to confirm the Ag NPs loading on Zn-MOF. EDS-mapping for Ag NPs/Zn-MOF nanocomposites is presented in Fig. 4a–c. It clearly shows that the Ag NPs is uniformly distributed and successfully loaded on the surface of Zn-MOF.

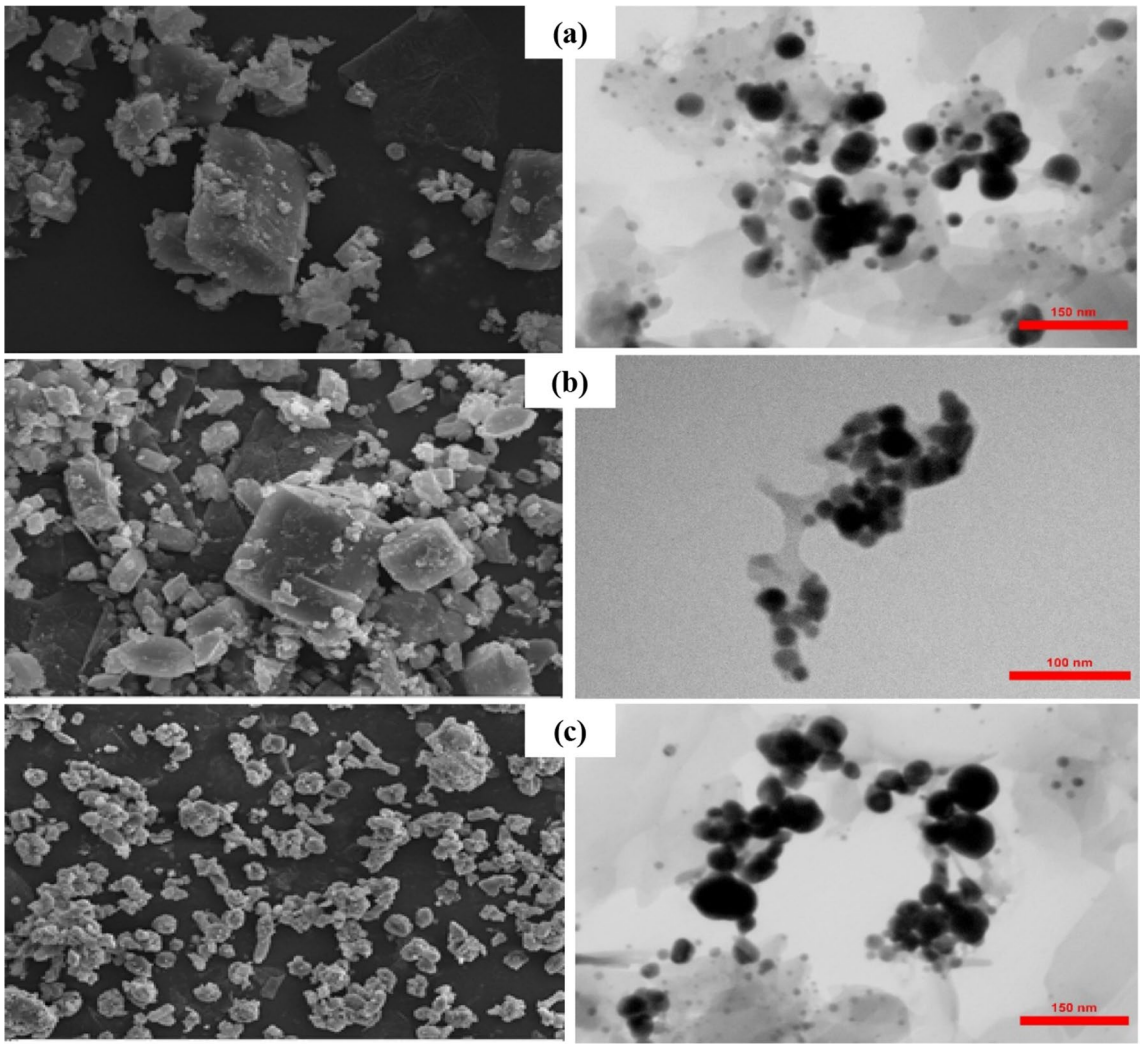

Fig. 3 SEM and TEM images of **a** Ag NPs/Zn-MOF **1**, **b** Ag NPs/Zn-MOF **2**, and **c** Ag NPs/Zn-MOF **3** nanocomposites

3.2 Evaluation of the Antibacterial Activity

The results of the antibacterial activity study of the synthesized nanocomposites are shown in Table 1. The growth inhibition that Ag NPs/Zn-MOF **1** and Ag NPs/Zn-MOF **2** displayed against tested microorganisms was greater than that of pristine Zn-MOF. However, the growth inhibition activity of Ag NPs/Zn-MOF **3** was not appreciably different from that of Zn-MOF. Ag NPs/Zn-MOF **1** revealed a broad-spectrum of antibacterial activity, so that all the tested strains were sensitive to this nanocomposite. It was also observed that *S. aureus* ATCC 6538 and *B. subtilis* ATCC 6633 were the most sensitive bacteria to Ag NPs/Zn-MOF **1** and, in the same time, the most resistant to Zn-MOF nanomaterials, Moreover, Ag NPs/Zn-MOF nanocomposites displayed dose-dependent antibacterial activity against all the four tested bacterial strains which is likely due to the slow release of silver ions from the Ag NPs/Zn-MOFs. The higher antimicrobial activity of Ag NPs/Zn-MOFs compared to the pristine Zn-MOF might be attributed to the released of silver ions from the surface of Ag NPs/Zn-MOFs. These ions then interact with the sulfur, oxygen, and nitrogen atoms of the essential biological molecules that support bacterial life. The alternative mechanism of consideration can be the interaction of Ag NPs with the bacterial cells and disrupting of the membrane which finally resulting in the destruction of the bacteria [28, 29].

4 Conclusion

In this research, Ag NPs/Zn-MOFs nanocomposites were successfully prepared through a straightforward multistep procedure. PXRD analysis revealed the presence of Ag nanoparticles onto the Zn-MOF matrix. The size of the Ag NPs and their uniform distribution in the as-prepared Ag

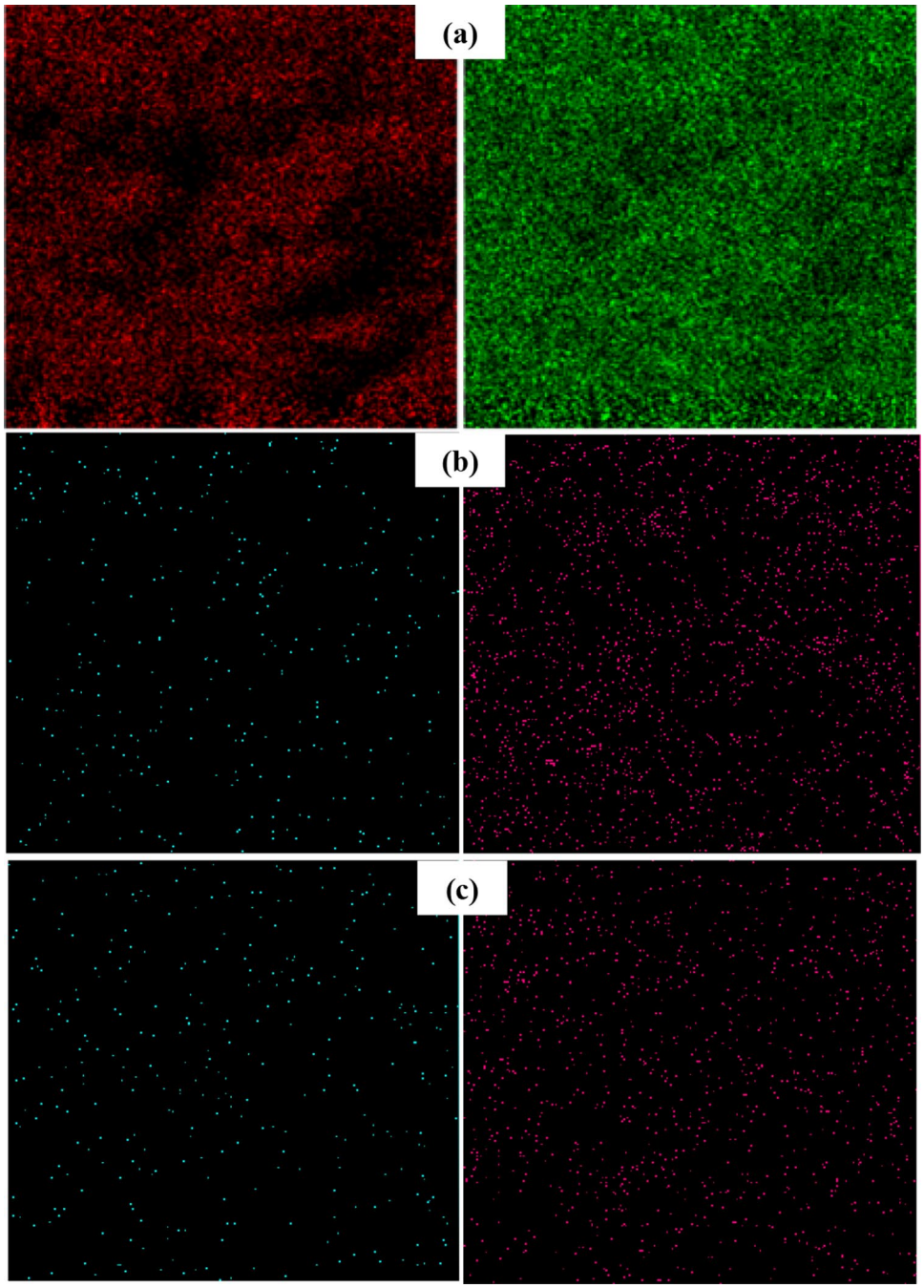

Fig. 4 Zn and Ag elemental mapping of **a** Ag NPs/Zn-MOF **1**, **b** Ag NPs/Zn-MOF **2**, and **c** Ag NPs/Zn-MOF **3** nanocomposites

NPs/Zn-MOF nanocomposites were clearly determined by TEM and EDS-mapping analyses, respectively. The antibacterial activity of the pristine Zn-MOF and Ag NPs/Zn-MOFs nanocomposites were evaluated against some gram-positive and gram-negative bacteria. Our findings showed that Ag NPs/Zn-MOF **1** nanocomposite, which contains higher amount of Ag NPs, exhibits broad-spectrum antibacterial activity. The results of this study are encouraging and Ag NPs loaded Zn-MOF composite can be considered as a potential scaffold for the development of promising antibacterial agents.

Table 1 Antibacterial activity of Ag NPs/Zn-MOF nanocomposites

Compound	Conc. (mg mL^{-1})	Inhibition zone (mm)			
		E. coli	*P. aeruginosa*	*S. aureus*	*B. subtilis*
Zn-MOF	1	R	R	8	R
	2	R	R	9	R
	4	R	R	9	R
	8	R	R	9	R
1	1	8	8	9	R
	2	9	9	10	R
	4	10	9	10	8
	8	11	9	12	9
2	1	R	R	R	R
	2	8	R	9	R
	4	9	R	9	R
	8	9	R	10	R
3	1	R	R	R	R
	2	R	R	8	R
	4	R	R	9	R
	8	R	R	9	R

R resistant

Acknowledgements The authors gratefully acknowledge the financial support (Grant No.: SCU.SC.98.20911) from the Shahid Chamran University of Ahvaz, Iran.

References

1. B. Li, J.G. Ma, P. Cheng, Integration of metal nanoparticles into metal–organic frameworks for composite catalysts: design and synthetic strategy. Small **15**, 1804849 (2019)
2. M. Azharuddin, G.H. Zhu, D. Das, E. Ozgur, L. Uzun, A.P. Turner, H.K. Patra, A repertoire of biomedical applications of noble metal nanoparticles. Chem. Commun. **55**, 6964–6996 (2019)
3. P. Velmurugan, S.-M. Lee, M. Iydroose, K.-J. Lee, B.-T. Oh, Pine cone-mediated green synthesis of silver nanoparticles and their antibacterial activity against agricultural pathogens. Appl. Microbiol. Biotechnol. **97**, 361–368 (2013)
4. D. Liu, J. Pan, J. Tang, W. Liu, S. Bai, R. Luo, Ag decorated SnO_2 nanoparticles to enhance formaldehyde sensing properties. J. Phys. Chem. Solids **124**, 36–43 (2019)
5. S. Hassanpour, M. Hasanzadeh, A. Saadati, N. Shadjou, J. Soleymani, A. Jouyban, A novel paper based immunoassay of breast cancer specific carbohydrate (CA 15.3) using silver nanoparticles-reduced graphene oxide nano-ink technology: a new platform to construction of microfluidic paper-based analytical devices (μPADs) towards biomedical analysis. Microchem. J. **146**, 345–358 (2019)
6. V. Ambrogi, D. Pietrella, A. Donnadio, L. Latterini, A. Di Michele, I. Luffarelli, M. Ricci, Biocompatible alginate silica supported silver nanoparticles composite films for wound dressing with antibiofilm activity. Mater. Sci. Eng. C **112**, 110863 (2020)
7. S. Mortazavi-Derazkola, M.A. Ebrahimzadeh, O. Amiri, H.R. Goli, A. Rafiei, M. Kardan, M. Salavati-Niasari, Facile green synthesis and characterization of Crataegus microphylla extract-capped silver nanoparticles (CME@Ag-NPs) and its potential antibacterial and anticancer activities against AGS and MCF-7 human cancer cells. J. Alloy. Compd. **820**, 153186 (2020)
8. B. Chen, Y. Jiang, M. Zhao, W. Wang, Z. Chu, R. Huo, F. Hu, W. Zhou, T. He, H. Qian, Ag nanoparticles decorated hybrid microspheres for superior antibacterial properties. Mater. Lett. **262**, 127057 (2020)
9. A. Phuruangrat, S. Siri, P. Wadbua, S. Thongtem, T. Thongtem, Microwave-assisted synthesis, photocatalysis and antibacterial activity of Ag nanoparticles supported on ZnO flowers. J. Phys. Chem. Solids **126**, 170–177 (2019)
10. H. Veisi, S. Kazemi, P. Mohammadi, P. Safarimehr, S. Hemmati, Catalytic reduction of 4-nitrophenol over Ag nanoparticles immobilized on *Stachys lavandulifolia* extract-modified multi walled carbon nanotubes. Polyhedron **157**, 232–240 (2019)
11. G. Ipek Yucelen, R.E. Connell, J.R. Terbush, D.J. Westenberg, F. Dogan, Synthesis and immobilization of silver nanoparticles on aluminosilicate nanotubes and their antibacterial properties. Appl. Nanosci. **6**, 607–614 (2016)
12. S.S. Gasaymeh, N.N. ALmansoori, Novel formation mechanism of Ag/PANI/PVP core-shell nanocomposites. Result. Phys. **16**, 102882 (2020)
13. V.V. Karve, D.T. Sun, O. Trukhina, S. Yang, E. Oveisi, J. Luterbacher, W.L. Queen, Efficient reductive amination of HMF with well dispersed Pd nanoparticles immobilized in a porous MOF/polymer composite. Green Chem. (2020). https://doi.org/10.1039/C9GC03140E
14. X. Li, Z. Zhang, W. Xiao, S. Deng, C. Chen, N. Zhang, Mechanochemistry-assisted encapsulation of metal nanoparticles in MOF matrices via a sacrificial strategy. J. Mater. Chem. A **7**, 14504–14509 (2019)
15. Y. Han, H. Xu, Y. Su, Z. Xu, K. Wang, W. Wang, Noble metal (Pt, Au@Pd) nanoparticles supported on metal organic framework (MOF-74) nanoshuttles as high-selectivity CO_2 conversion catalysts. J. Catal. **370**, 70–78 (2019)
16. P.V. Baptista, M.P. McCusker, A. Carvalho, D.A. Ferreira, N.M. Mohan, M. Martins, A.R. Fernandes, Nano-strategies to fight multidrug resistant bacteria-"a battle of the titans". Front. Microbiol. **9**, 1441 (2018)
17. G. Wyszogrodzka, B. Marszalek, B. Gil, P. Dorozynski, Metal-organic frameworks: mechanisms of antibacterial action and potential applications. Drug Discov Today **21**, 1009–1018 (2016)
18. N. Bhardwaj, S.K. Pandey, J. Mehta, S.K. Bhardwaj, K.-H. Kim, A. Deep, Bioactive nano-metal–organic frameworks as antimicrobials against gram-positive and gram-negative bacteria. Toxicol. Res. **7**, 931–941 (2018)
19. S.G. Surya, S. Bhanoth, S.M. Majhi, Y.D. More, V.M. Teja, K.N. Chappanda, A silver nanoparticle-anchored UiO-66(Zr) metal–organic framework (MOF)-based capacitive H_2S gas sensor. CrystEngComm **21**, 7303–7312 (2019)
20. R. Mahugo, A. Mayoral, M. Sánchez-Sánchez, I. Diaz, Observation of Ag nanoparticles in/on Ag@MIL-100(Fe) prepared through different procedures. Front. Chem. **7**, 686 (2019)
21. D.M. Ciurtin, Y.-B. Dong, M.D. Smith, T. Barclay, Z. Loy, Two versatile N,N′-bipyridine-type ligands for preparing organic–inorganic coordination polymers: new cobalt- and nickel-containing framework materials. Inorg. Chem. **40**, 2825–2834 (2001)
22. V. Safarifard, S. Beheshti, A. Morsali, An interpenetrating amine-functionalized metal–organic framework as an efficient and reusable catalyst for the selective synthesis of tetrahydro-chromenes. CrystEngComm **17**, 1680–1685 (2015)
23. A. Mirzaie, T. Musabeygi, A. Afzalinia, Sonochemical synthesis of magnetic responsive Fe_3O_4@TMU-17-NH_2 composite as

sorbent for highly efficient ultrasonic-assisted denitrogenation of fossil fuel. Ultrason. Sonochem. **38**, 664–671 (2017)
24. M. Yadollahi, H. Hamadi, V. Nobakht, $CoFe_2O_4$/TMU-17-NH_2 as a hybrid magnetic nanocomposite catalyst for multicomponent synthesis of dihydropyrimidines. Appl. Organomet. Chem. **33**, e4629 (2019)
25. M. Govarthanan, T. Selvankumar, K. Manoharan, R. Rathika, K. Shanthi, K.J. Lee, M. Cho, S. Kamala-Kannan, B.T. Oh, Biosynthesis and characterization of silver nanoparticles using panchakavya, an Indian traditional farming formulating agent. Int. J. Nanomed. **9**, 1593–1599 (2014)
26. K. Jyoti, M. Baunthiyal, A. Singh, Characterization of silver nanoparticles synthesized using *Urtica dioica* Linn. leaves and their synergistic effects with antibiotics. J. Radiat. Res. Appl. Sci. **9**, 217–227 (2016)
27. Y. Cai, X. Piao, W. Gao, Z. Zhang, E. Nie, Z. Sun, Large-scale and facile synthesis of silver nanoparticles via a microwave method for a conductive pen. RSC Adv. **7**, 34041–34048 (2017)
28. C. Cermelli, A. Fabio, G. Fabio, P. Quaglio, Effect of eucalyptus essential oil on respiratory bacteria and viruses. Curr. Microbiol. **56**, 89–92 (2008)
29. M.J. Hajipour, K.M. Fromm, A. Akbar Ashkarran, D.J. de Aberasturi, I.R. Larramendi, T. Rojo, V. Serpooshan, W.J. Parak, M. Mahmoudi, Antibacterial properties of nanoparticles. Trends Biotechnol. **30**, 499–511 (2012)